ACS Photonics

Article

pubs.acs.org/journal/apchd5

Macroscopic Layers of Chiral Plasmonic Nanoparticle Oligomers from Colloidal Lithography

Robin Ogier,[†] Yurui Fang,[†] Mikael Svedendahl,[†] Peter Johansson,[†,‡] and Mikael Käll*[,†]

[†]Department of Applied Physics, Chalmers University of Technology, S412 96 Göteborg, Sweden

[‡]School of Science and Technology, Örebro University, S701 82 Örebro, Sweden

Supporting Information

ABSTRACT: Optical near-field coupling between closely spaced plasmonic metal nanoparticles is important to a range of nanophotonic applications of high contemporary interest, including surface-enhanced molecular spectroscopy, nanooptical sensing, and various novel light-harvesting concepts. Here we report on monolayers of chiral heterotrimers and heterotetramers composed of closely spaced silver and/or gold nanodisks of different heights fabricated through facile hole-mask colloidal lithography. These quasi-three-dimensional oligomers are interesting for applications because they exhibit "hot" gaps and crevices of nanometric dimensions, a pronounced circular dichroism, and optical chirality in the visible to near-infrared wavelength range, and they can be produced in large ensembles (>10^9) of identical orientation. We analyze the optical properties of the samples based on simulation results and find that the circular dichroism is due to strong near-field coupling and intricate phase retardation effects originating in the three-dimensional character of the individual oligomers.

KEYWORDS: *plasmonics, optical chirality, circular dichroism, hole-mask colloidal lithography, oligomers, numerical simulation*

Chiral atomic structures, that is, structures that possess a certain sense of rotation, left or right, are ubiquitous in nature. One of the most subtle but important consequences of this structural property is optical activity, that is, the phenomenon that a chiral material can rotate the polarization of light or, equivalently, that the optical constant characterizing the material is different for left-handed and right-handed circularly polarized light (LCP and RCP, respectively).[1] Many biomolecules, including essential amino acids, nucleic acids, and many proteins, exhibit optical activity due to a well-defined chirality that is crucial to their chemical function. Other biological structures, such as the cuticles of certain beetles,[2] exhibit chirality and optical activity for no apparent reason. Optical activity can sometimes be revealed by just viewing the chiral material through circular polarizers, such as the eyeglasses provided for some 3D movies. This is, for example, the case for the chiral beetle wings mentioned above, which exhibit different color and brightness for LCP and RCP light.[3] However, molecular optical activity is in general a weak effect that requires large sample volumes for quantitative analysis based on traditional measurement techniques, such as circular dichroism (CD), optical rotatory dispersion (ORD), or Raman optical activity (ROA).[4] The importance of such analysis, for example in drug development, has motivated research into more sensitive methods, including nonlinear[5] and microwave spectroscopies,[6] and novel concepts, such as utilizing local "superchiral" fields for selectively exciting left-handed or right-handed molecular enantiomers.[7,8]

The past decade has seen a surge of interest in artificial nanostructures and metamaterials that exhibit optical activity. Most of this attention has focused on metal nanostructures that support various kinds of surface plasmon resonances since plasmonic structures have the potential to become key elements in a wide range of future technologies based on optical near-field effects.[9−11] Early investigations primarily considered planar metal structures, like two-dimensional (2D) gammadions, which exhibit optical activity for oblique illumination,[12,13] while a number of recent investigations have focused on achieving optical activity in three-dimensional (3D) helical nanostructures of various forms,[14−17] including oligomers of gold nanodisks.[18] Surface-bound chiral nanostructures produced through bottom-up lithography over large areas may turn out to be crucial to applications.[19,20] Optical activity can also result from the combination of chiral molecules with metal structures.[21] In particular, several reports have demonstrated that coupling between intrinsically achiral metal nanostructures, like colloidal gold particles, and chiral molecules can lead to a dramatically enhanced optical activity.[22−29]

Surface plasmons are well known for their ability to amplify optical signals from molecules residing within nanometric distances from the metal surface through electric field enhancement effects, the most well-known applications thereof

Received: August 7, 2014
Published: September 22, 2014

being surface-enhanced Raman scattering (SERS)[30] and surface plasmon resonance (SPR) sensing.[31] It is therefore not surprising that many of the above-mentioned reports have been motivated from a plasmon-enhanced molecular analysis perspective, to be specific, by the possibility to distinguish molecular enantiomers with higher sensitivity than what can be achieved by current analysis methods. Indeed, a surface-enhanced version of ROA (SEROA) was reported several years ago,[32] although a detailed understanding of the experimental results is still lacking.[33] Moreover, recent reports on enhanced CD of biomacromolecules interfaced to 2D plasmonic gammadions[34] and of LCP-RCP fluorescence excitation dissymmetry of dye molecules attached to chiral nanoplasmonic structures[35] highlight the possibility of utilizing "superchiral" plasmonic near-fields for molecular analysis.[36−39]

RESULTS AND DISCUSSION

In this article, we report on the optical properties of chiral plasmonic nanoparticle oligomers fabricated over cm^2 areas using facile hole-mask colloidal lithography (HCL).[40] The oligomer consists of closely spaced or slightly overlapping gold and/or silver disks with different height to diameter aspect ratios and a strong optical response in the visible to near-infrared wavelength range. Several reports have demonstrated that the optical activity of chiral particle arrangements critically depends on the strength of interparticle interactions; that is, strong near-field coupling and plasmon hybridization dramatically enhance optical activity.[41−43] We analyze the complex CD spectra of a tetramer structure using electrodynamic simulations and a simplified coupled-dipole model and find that this is indeed the case also for the present system. It is well known that strong particle interactions can lead to enormous field enhancement in gaps or crevices between particles and result in a dramatic amplification of molecular optical cross sections, such as in single-molecule SERS.[44,45] Similar effects might be expected for molecular analysis based on "superchiral" fields generated in the vicinity of plasmonic nanostructures.[46] Since the average gap distance between the individual nanodisks in our oligomers can be as small as a few nanometers, and the gaps are readily accessible for molecular binding reactions, the structures should be well adapted for various molecular spectroscopy and sensing applications.

Figure 1A gives an overview of the fabrication method used. As detailed in the Methods section, we employ a variant of HCL based on an off-normal evaporation angle (typically on the order of 10−15 deg relative to the substrate normal) and subsequent rotation of the substrate in steps of $360/N$ deg between evaporations in order to create millions of identically oriented oligomers, each consisting of N disk-like nanoparticles, on a substrate. The same method has recently been used to fabricate metal heterodimers ($N = 2$) for color routing and H_2-gas sensing.[47,48] Figure 1B−D illustrate the wide varieties of chiral samples that can be produced: Figure 1B and C show left-handed gold (LH) and right-handed silver (RH) tetramers, respectively, Figure 1D a gold trimer, and Figure 1E a gold tetramer with slightly overlapping particles. All samples were prepared on glass coverslips. Note that the individual particles have an essentially circular footprint but slightly different diameters. This comes about because the hole in the mask gradually shrinks in diameter as more material is evaporated. Thus, the last particles in a preparation typically have the smallest diameters, and thick particles typically acquire a slightly conical shape. However, the chirality in these samples mainly

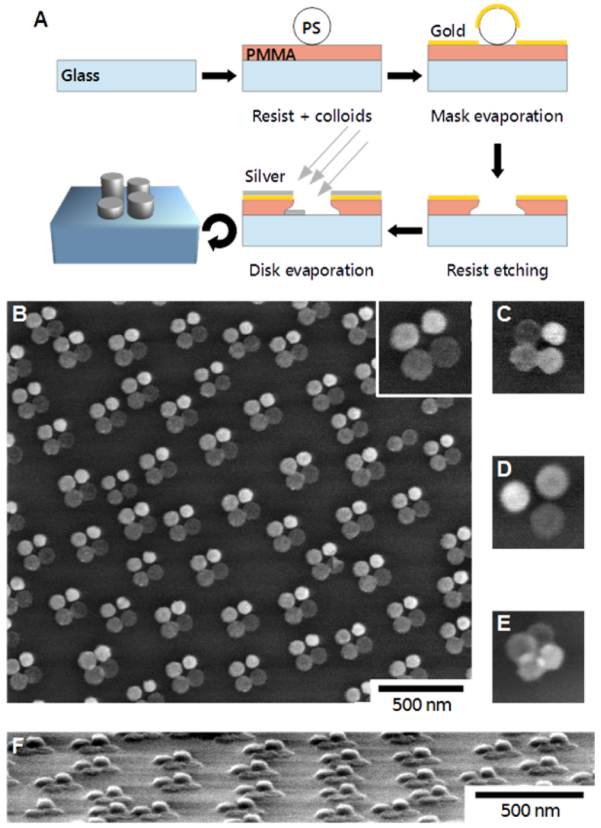

Figure 1. (A) Sample fabrication process illustrated for the case of silver tetramers. (B) SEM image of a substrate covered with left-handed (LH) gold tetramers. (C−E) Close-up SEM images of a right-handed (RH) silver tetramer, a RH gold trimer, and an overlapped RH gold tetramer. The different shades of gray correspond to nanodisks with height 40 nm (brightest), 30, 20, and 10 nm (darkest). The nanodisks have maximum diameters on the order of 100 nm. (F) Side-view SEM image that illustrates the staircase-like 3D character of the oligomers.

stems from the different heights of the individual nanodisks, which are 40, 30, 20, and 10 nm for the whitish, light gray, medium gray, and dark gray particles in the scanning electron microscopy (SEM) images, respectively. Thus, each oligomer is a quasi-3D object, which is also evident from the side-view SEM image shown in Figure 1F. Note also that individual oligomers in a single sample vary somewhat in the gap size or degree of disk overlap, as can be seen from Figure 1A. This is due to a variation in the diameter of the individual holes in the hole-mask, caused by a slight polydispersity (of the order of 8%) of the colloidal polystyrene (PS) beads, and results in inhomogeneous broadening of corresponding ensemble-averaged oligomer spectra.

Samples made by HCL do not exhibit long-range translation order since PS beads attach to the substrate in a more or less random fashion and the interbead forces are weakly repulsive. However, as might be seen from Figure 1B, there is a quite well-defined nearest-neighbor distance between oligomers, which is on the order of 400 nm for the samples discussed here. Hence, for light incident normal to the sample surface, which is what we consider below, and for the investigated wavelength range, which was ∼450−900 nm, we do not expect any pronounced grating effects.[49] The comparatively large distances between individual oligomers also imply that optical near-field coupling between oligomers is reduced. Indeed,

dx.doi.org/10.1021/ph500293u | ACS Photonics 2014, 1, 1074−1081

previous investigations of HCL samples have demonstrated that normal-incidence transmission/extinction spectra are well described by uncoupled single-particle optical properties.[50]

We analyzed the samples under normal incidence using a home-built setup for transmission spectroscopy, as described in the Methods section. Optical extinction cross sections for individual oligomers were calculated by dividing the sample transmission spectra $T(\lambda)$ by the oligomer surface density n as measured from SEM images; that is, $\sigma_{ext} = (1 - T)/n$. Surface densities were on the order of $n \approx 8\ \mu m^2$, which means that a measurement averages over several million individual oligomers. We also calculated the classical measure of optical activity used in circular dichroism characterization of molecular species; that is, $\tan\theta = (T_{RCP}^{1/2} - T_{LCP}^{1/2})/(T_{RCP}^{1/2} - T_{LCP}^{1/2})$. The angle θ is a measure of the ellipticity acquired by linearly polarized light after passing through a chiral structure. It is then assumed that circularly polarized light transmitted through the structure largely remains circularly polarized, but that the transmission probability may be different for the two different circular polarization orientations. In the cases we consider here $\tan\theta \ll 1$, so that, measured in degrees, $\theta \approx (180/\pi)\tan\theta$.

Figure 2 displays exemplary RCP and LCP extinction cross-section spectra together with corresponding CD (θ) spectra for three different samples: gold trimers, overlapped gold tetramers, and heterometallic tetramers built from three gold disks and a single silver disk to illustrate the variety of structures that can be made by the described methodology. Original transmission spectra are presented in the Supporting Figures 1 and 2. Overall, the samples display similar optical characteristics. The maximum extinction cross sections, at the main plasmon peaks, are on the order of 3 to 4 times higher than the geometrical cross-section area and transmission values range between ~5% and ~90%. The largest relative extinction differences between RCP and LCP light is observed close to the plasmon peaks, where both $|\Delta T/\overline{T}|$ and $|\Delta\sigma/\overline{\sigma}|$ reach 5−6% (here $\Delta T = T_{LCP} - T_{RCP}$, $\overline{T} = (T_{RCP} + T_{LCP})/2$, etc.). From comparing the spectral shapes of the extinction curves, it is clear that these differences arise due to changes in both plasmon peak amplitude and peak position. The corresponding CD spectra consequently display both negative and positive values. However, the absolute θ values are difficult to read off directly from the extinction spectra because θ is a relative rather than an absolute measure of extinction differences. For small differences in extinction, we have $\theta\ [\text{deg}] \approx 14.3\Delta T/\overline{T} \approx -14.3\Delta\sigma/(n^{-1} - \overline{\sigma})$; that is, a certain extinction difference results in a larger CD angle when the overall extinction is high. Nevertheless, the θ values observed are high compared to most previous reports on chiral plasmonic nanostructures resonating in the investigated wavelength range.[9,26,51,52]

To get a better understanding of the basic mechanism behind the overall optical response of the oligomers, we now focus specifically on silver tetramers. We prepared both RH and LH samples, and the corresponding cross-section spectra for RCP and LCP light are displayed in Figure 3A and B, respectively. To visualize the relative extinction differences, we also plot the dissymmetry factor $g = \Delta T/\overline{T}$. As anticipated for chiral

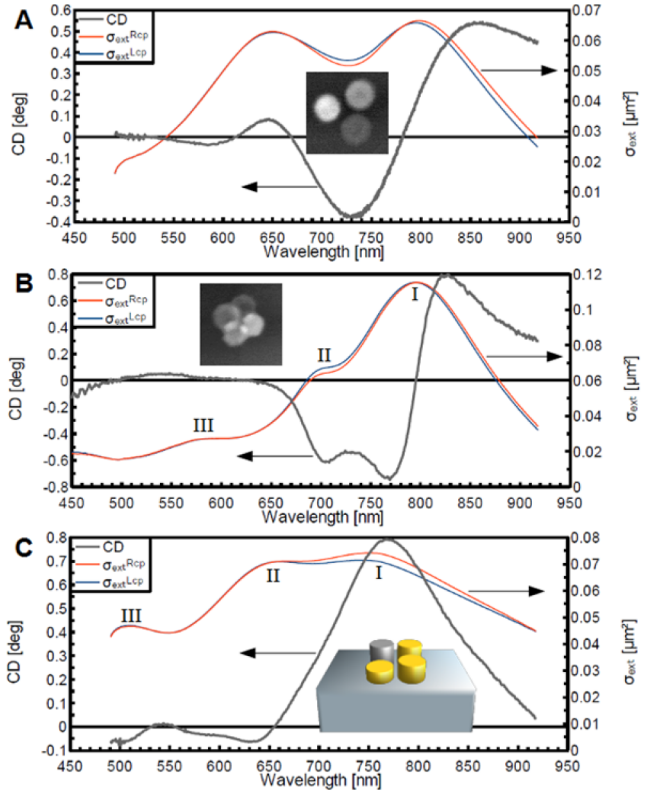

Figure 2. Illustration of optical properties of chiral nanodisk oligomers. The panels show extinction cross sections for RCP and LCP light and corresponding CD spectra for (A) RH gold trimers (surface density: 8.27 μm^{-2}), (B) overlapped RH gold tetramers (surface density: 7.38 μm^{-2}), and (C) heterometallic tetramers consisting of three gold disks, with heights 10, 20, and 30 nm, and one silver disk of height 30 nm (surface density: 7.79 μm^{-2}).

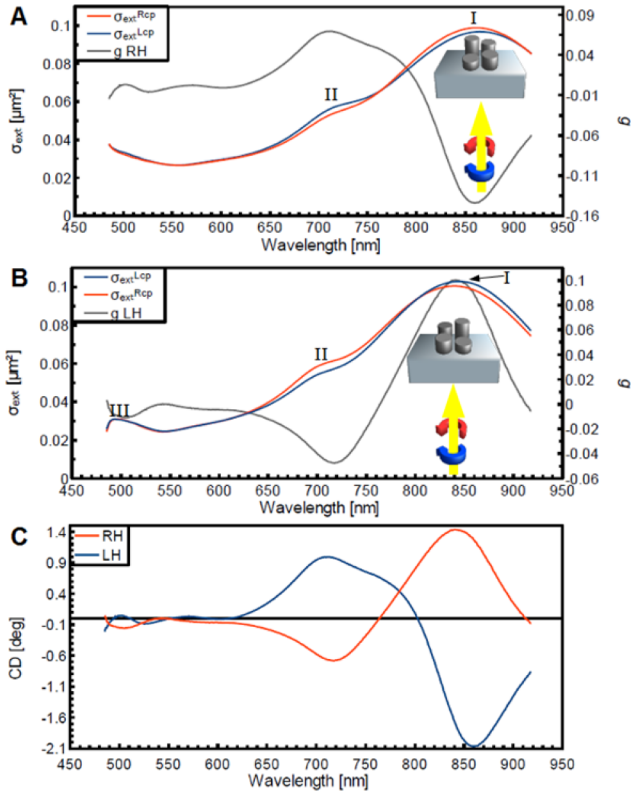

Figure 3. Experimental extinction cross sections for RCP (red) and LCP (blue) light, together with corresponding dissymmetry factors g, for (A) RH silver tetramers (surface density n = 8.16 μm^{-2}) and (B) LH silver tetramers (n = 8.07 μm^{-2}) together with (C) corresponding CD spectra for the RH (red) and LH (blue) samples.

dx.doi.org/10.1021/ph500293u | ACS Photonics 2014, 1, 1074−1081

enantiomers, the corresponding CD spectra, Figure 3C, are essentially mirror images of each other (small differences can be explained by small variations in the fabrication process); that is, the extinction (or transmission) spectrum for the RH structure probed by RCP/LCP light mimics that for the LH structure probed by LCP/RCP light. The mode structure and CD spectra observed for the silver tetramers are qualitatively similar to those for the overlapped gold tetramer and the heterometallic tetramer in Figure 2; that is, the spectra are dominated by a main plasmon peak in the deep red (peak I, 750−850 nm) flanked by a second peak in the red (peak II, 650−700 nm) and some weaker structures in the blue-green region of the spectra (peak III). We used two different simulation methods as a guide for interpretation of the optical response: the finite element method (FEM), which gives fully retarded solutions to Maxwell's equations, and the coupled dipole approximation (CDA), where each particle is represented by a point dipole with an effective polarizability obtained by solving the coupled dipole equation. The corresponding uncoupled dipole polarizabilities are obtained by approximating each disk by an oblate spheroid with similar dimensions to those in the real sample. The FEM model was based on cylindrical disks with the same heights as in the CDA (10, 20, 30, 40 nm) but with identical diameters of 100 nm. Both calculations were based on positioning the particles on a square base with a side length of 102 nm, that is, a gap size of 2 nm in the FEM simulations. All simulations assume a uniform surrounding medium of effective refractive index 1.25, i.e. in between that of the glass substrate and the air environment. The results of the simulations are displayed in Figure 4 and in Supporting Figures 3 and 4.

A comparison between the measured extinction spectra in Figure 3 and the simulated ones in Figure 4A and B shows that experiment and theory are in good qualitative agreement. In particular, both the CDA and the FEM simulations capture the overall structure of the spectra, with two main features in the red and weaker structure in the blue-green spectral region. Analysis of the induced charge distributions at the spectral peak positions from the FEM simulations and the spectral evolution as a function of interparticle distance in CDA (Supporting Figure 2) showed that the strong long-wavelength peaks, features I and II, are dominated by the in-plane dipolar plasmons of the 10 nm thin and 20 nm thin disks, respectively, while feature III contains a mixture of dipolar oscillations of the two taller disks and multipolar, in particular quadrupolar, contributions. These results are quite expected from the well-known variation in plasmon peak position with particle aspect ratio (that is, flatter disks resonate at longer wavelengths) and by the fact that a small spectral overlap between modes of the individual nanodisks in an oligomer can be expected to decrease the degree of plasmon hybridization. However, the particle interactions are certainly not negligible, which is evident from the strong charge accumulation in the gap regions between the individual disks in the FEM simulations (Supporting Figure 3). In the CDA model, on the other hand, each nanodisk is represented by a point dipole located at the center-of-mass coordinates of the associated disk. The CDA model therefore underestimates the near-field interactions, partly because of the artificially large interparticle distance and partly because multipolar interactions are neglected. This also explains why the CDA simulation underestimates the overall red-shift of the spectra (see Supporting Figure 2) compared to the FEM model.

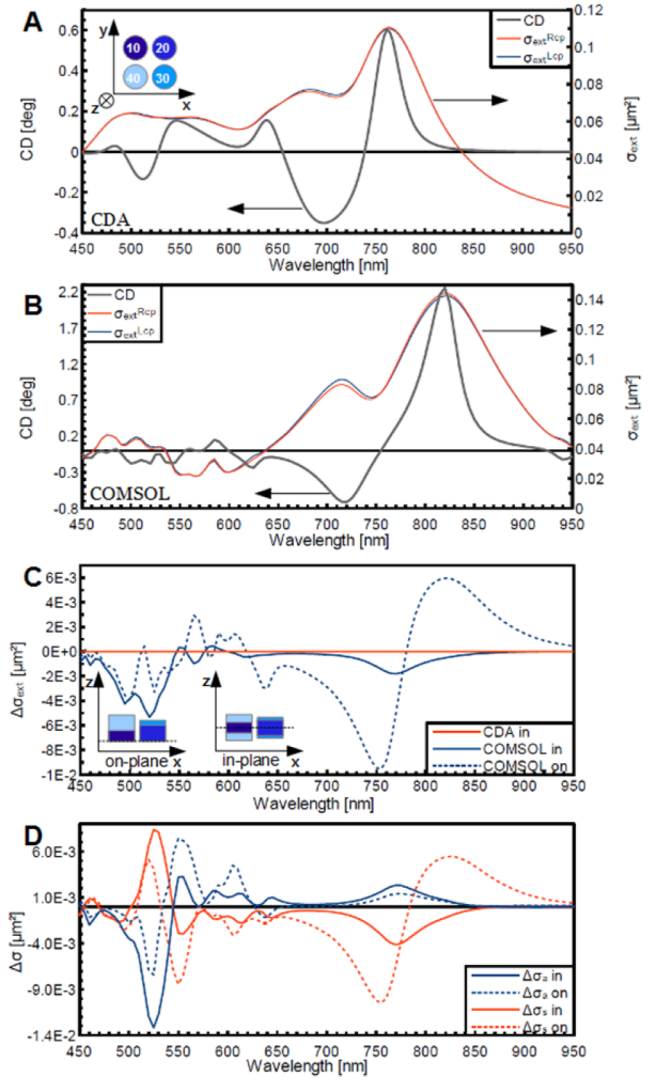

Figure 4. Simulated optical properties of right-handed silver tetramers based on the coupled dipole approximation (CDA) and the finite element method (FEM). (A) CDA simulation of extinction cross section for RCP and LCP light and corresponding CD spectrum based on a tetramer surface density of $n = 8\ \mu m^{-2}$ and a uniform surrounding refractive index of $n = 1.25$. (B) Same as in A, but using FEM for tetramer in a vacuum ($n = 1$) on a glass ($n = 1.5$) substrate. (C) Simulated differences in extinction between RCP and LCP light for a tetramer in a uniform medium ($n = 1.25$) and organized in the "in-plane" and "on-plane" configurations based on CDA and FEM. (D) Absorption and scattering contributions to the RCP/LCP extinction cross-section differences shown in C.

The CD signal in Figure 2 and Figure 3 originates from, in general, very small differences in extinction of RCP and LCP light, and it is therefore difficult to explain the spectral structure in detail. However, a reasonable qualitative understanding can be reached. We first notice that the RH structures all exhibit a dominant CD feature consisting of a dip in the red followed by a strong peak in the deep red. This feature results from a slight plasmon red-shift (signaling stronger near-field coupling) and amplitude increase (signaling a stronger coupling to the incident field) of the two main plasmon resonances (peaks I and II) when probed with RCP light compared to the LCP case. Thus, the optical interactions are stronger when the RH structure is excited with RCP than with LCP light, and vice

dx.doi.org/10.1021/ph500293u | ACS Photonics 2014, 1, 1074−1081

versa for an LH structure. This interpretation is in agreement with previous studies of plasmonic chiral nanostructures and can be qualitatively thought of as the result of an interaction of induced electric and magnetic (circular current) dipoles, with the same handedness as the incident light, which is hindered or facilitated by the twist of the structure. This effect cannot occur when the particles in an oligomer are far apart, but the particles do not need to be in direct metallic contact since we are dealing with an ac current characterized by exceedingly small charge displacements. Consequently, the magnitude of the CD signals observed for slightly overlapped oligomers, such as the one in Figure 2C, is not much different than that for structures with small but distinct gaps (e.g., the trimer in Figure 2B). The silver tetramer samples in Figure 3 contained a mixture of gapped and slightly overlapped oligomers, resulting in evenly broadened spectral features.

The importance of interactions for the CD amplitude was evident from the FEM simulations but can also be seen from the CDA results (Supporting Figure 2). However, a strong interparticle interaction is not the only prerequisite for a strong CD signal in a chiral oligomer structure: the individual particles also have to be arranged in 3D such that space and time inversion symmetry along the light propagation direction is broken. In other words, a completely 2D system does not exhibit CD. This is a general result for any collection of scatterers, chiral or not, confined to a plane. When illuminated by a circularly polarized wave at normal incidence, the forward scattered signal, which in accordance with the optical theorem determines the extinction cross-section, is the same for both polarization twists. However, the polarization in different parts of the structure can vary a lot between the two cases. Hence, the absorption cross section of a composite 2D structure can differ for RCP and LCP light, but such a difference has to be offset by the corresponding scattering cross sections to keep the net extinction cross section constant. In Figure 4B and C, we investigate these rather subtle effects using CDA and FEM simulations of two different types of RH tetramers: an *on-plane* tetramer and an *in-plane* tetramer. The on-plane tetramer corresponds to the regular geometry we have considered so far; that is, the base of all disks are on the same plane (corresponding to the substrate in the experiments). In the in-plane tetramer, in contrast, we have positioned the center-of-mass of each disk in the same plane. Results are displayed as $\Delta\sigma$, that is, the difference in cross-section between RCP and LCP light. We first note that the CDA $\Delta\sigma$ spectrum for the in-plane structure vanishes everywhere, whereas that based on the FEM simulation does not. This is in agreement with the discussion above: the CDA model is based on point dipoles and therefore is strictly 2D, while the finite spatial extension of the nanodisks along the light propagation direction in the more realistic FEM simulation introduces phase retardations and true 3D chirality that results in a small but finite chiral response. However, the CD effect is obviously much stronger in the on-plane case, corresponding to the experimental structures, which exhibits a much more pronounced 3D character. Finally, in Figure 4C, we have split up the FEM extinction differences $\Delta\sigma_e$ for the in-plane and on-plane structures into the corresponding absorption $\Delta\sigma_a$ and scattering $\Delta\sigma_s$ contributions. We see that the absorption and scattering features appear almost in the same spectral positions, but with different signs. For the in-plane case, the magnitudes of the two contributions are similar, which thus means that they almost cancel out in the composite $\Delta\sigma_e$ spectrum, as discussed above. Interestingly, this effect is particularly pronounced for the short-wavelength region dominated by quadrupolar resonances. Going instead to the on-plane case, one finds that the absorption contribution has decreased while the scattering has increased, resulting in a large amplification of the CD response in accordance with the plots in Figure 4B. From this, one can conclude that scattering effects dominate the CD response of the investigated structures, which is not unexpected considering the rather large overall volume of the oligomer structures.

As discussed in the introduction, one of the main arguments for investigating plasmonic structures with nanometric gaps or crevices is the possibility of generating "hot spots" with high electromagnetic field enhancement for various molecular spectroscopy applications. In the present context, the perspective of inducing so-called superchiral fields is particularly interesting. We simulated the *optical chirality*, as introduced by Tang and Cohen,[7] in the near-field around a tetramer using FEM. The optical chirality can be calculated as $C = -\varepsilon_0/2\omega\mathrm{Im}[\mathbf{E}^*\cdot\mathbf{B}]$ and quantifies the dissymmetry in excitation rate between LH and RH molecules. In Figure 5, we show the optical chirality enhancement factor in cuts through the "hot" gap regions and for a wavelength near the maximum CD response of the structure. The enhancement is calculated as $C/|C_{CP}|$, where $C_{CP} = \pm\varepsilon_0/2c\omega E_0^2$ is the optical chirality for a right (−) or left (+) circularly polarized plane wave with electric field amplitude E_0. It is clear that the strong field enhancement in the gaps (see Supporting Figure 4) also results in an enhancement of optical chirality, which reaches values on the order of 200−300 at favorable positions and wavelengths (see also Supporting Figure 5 for the case of λ = 880 nm). However, the gap regions are also characterized by rapid sign changes of C, such that the volume-integrated enhancement tends to cancel out. In molecular analysis experiments, where molecules are generally distributed randomly over the probe volume, the enhancement of the molecular excitation rate at one location then would tend to be compensated by a decrease at another location. We therefore also quantified the averaged optical chirality by integrating the enhancement factor in a 2 nm thick shell outside the metal surface to simulate the response of a molecular monolayer formed over the exposed part of the gold tetramer; see Figure 5D (and Supporting Figure 6 for the case of a larger averaging volume). As expected, the enhancement is now much reduced but still reaches values of ∼5 near the peak in the CD response. This should result in a quite clear difference in, for example, fluorescence or Raman excitation rates of achiral molecules for incident LCP vs RCP laser light.[35] It would be considerably more difficult to directly observe the CD of an enantiomerically enriched molecular layer, because even in the presence of the superchiral field enhancement, the difference in molecular absorbance between RCP and LCP would have to be resolved against the large intrinsic CD of the oligomers themselves. As discussed by Hendry et al.,[34] an interesting alternative is then to simply trace the variation in oligomer CD as a chiral molecular layer is formed on the metal surface, similar to what is done in standard surface plasmon resonance sensing experiments. This approach then assumes that the plasmon−molecule coupling depends on molecular chirality and is somehow enhanced by the superchiral near-fields.

In summary, we have demonstrated a versatile fabrication route for producing large areas of chiral trimer and tetramer nanostructures with pronounced circular dichroism. The particles in an individual oligomer all have disk-like shapes, but they can be made of different materials and have different

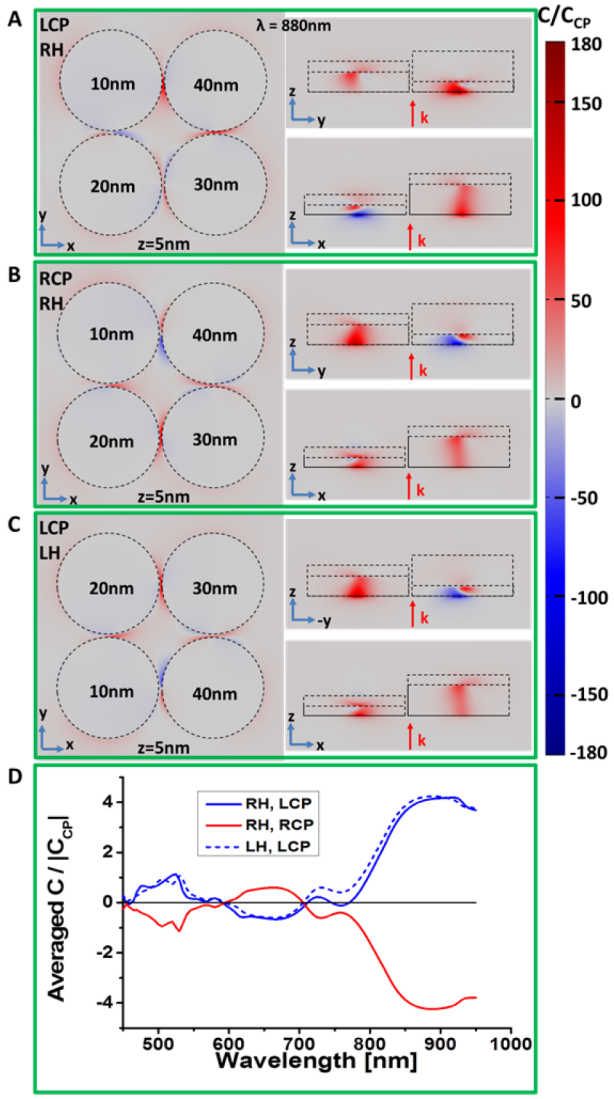

Figure 5. Simulated optical chirality enhancement factor of silver tetramers in a vacuum on a glass substrate based on the finite element method (FEM). (A) Optical chirality enhancement factor at 880 nm of a RH tetramer for LCP light and (B) RCP light. (C) Same as in A, but for a LH tetramer. (D) Averaged enhancement factor in a 2 nm thick shell surrounding the exposed metal surface.

heights. Because of the "gapped" nature of the structures, which results in strong electric field enhancement and optical chirality, the structures could be interesting to a wide range of applications. The chiral optical response of the structures results from a complicated interplay between optical near-field interactions and phase retardation within the three-dimensional oligomer structures.

METHODS

Sample Fabrication. Samples were prepared on cover glass substrates (Menzel-Gläser #2) spin coated with PMMA-A4 (MicroChem) and baked at 180 °C. A surfactant allows charged PS beads (Sigma-Aldrich) to attach at a surface density that can be controlled through the salinity of the PS bead solution. Evaporating a 10 nm thin gold film and then removing the PS beads by tape stripping create the hole-mask. Etching in an oxygen plasma digs out the hole, and subsequent metal evaporation at a specific angle builds a disk-like particle on the substrate, as indicated in Figure 1A. In the tetramer case, the substrate is then rotated in 90 deg increments to allow for evaporation of a second, a third, and a fourth disk. A final lift-off and rinse step completes the sample fabrication.

Transmission Spectroscopy. Samples were measured using collimated white light from a fiber-coupled halogen lamp (Ocean Optics HL-2000). The light beam was passed through a linear polarizer and an achromatic quarter wave plate (Thorlabs AQWP05M-630) tuned to obtain RCP or LCP light. The wave plate exhibits a relatively constant retardation within the 450−800 nm spectral range. We took great care to exactly align the sample normal to the light propagation direction. We estimated the alignment uncertainty to be around 0.25°, which has negligible spectral influence. The transmitted light was analyzed by a fiber-coupled grating spectrometer (BW-Tek BRC711E) equipped with appropriate collection optics. The sampling area was ∼10 mm^2, which encompasses tens of millions of individual oligomers. Spectra acquired with substrate side and nanostructure side facing the incident light differed only slightly; see Supporting Figure 1 for an example. Data displayed in Figures 2 and 3 were obtained for light incident on the substrate side of the samples. CD spectra calculated from transmission measurements were found to be in excellent agreement with those obtained using a commercial CD spectrometer (Jasco J810); see Supporting Figure 7.

Electrodynamics Simulations. Numerical simulations of optical properties were performed using a commercially available implementation of the FEM (COMSOL Multiphysics 3.5a) and tabulated values for the complex dielectric function of silver.[53] A tetramer was represented as four cylindrical disks with the same diameter (100 nm) but varying height (10, 20, 30, or 40 nm) arranged in a left-handed or right-handed fashion at the corner of a square either on a glass surface (n = 1.5) or in a uniform medium (n = 1.25). The tetramer was excited by a RCP or LCP plane wave entering from the substrate side. Differential scattering and absorption cross sections were obtained by integrating the far-field scattering over all angles and by integrating the dissipated energy inside the disks, respectively. Dipole simulations were based on solving the coupled dipole equation for interacting point dipoles using quasi-static polarizabilities for oblate spheroids with size corrections according to the modified long wavelength approximation.[54] The diameter/height values for the four particles in the tetramer were 100/10, 99/20, 88/30, and 76/40.

ASSOCIATED CONTENT

Supporting Information

Experimental transmission spectra, simulated extinction cross sections, near-field enhancement, and optical chirality enhancement factors are provided in the Supporting Information. This material is available free of charge via the Internet at http://pubs.acs.org.

AUTHOR INFORMATION

Corresponding Author

*E-mail: kall@chalmers.se.

Notes

The authors declare no competing financial interest.

■ ACKNOWLEDGMENTS

This work was supported by the Knut and Alice Wallenberg Foundation, the Swedish Foundation for Strategic Research (SSF), and the Chalmers Nanoscience and Nanotechnology Area of Advance.

■ REFERENCES

(1) Hecht, E. *Optics*, 4th ed.; Addison-Wesley, 2002; p 680.
(2) Michelson, A. A. On Metallic Colouring in Birds and Insects. *Philos. Mag.* **1911**, *21*, 554−567.
(3) Arwin, H.; Magnusson, R.; Landin, J.; Järrendahl, K. Chirality-Induced Polarization Effects in the Cuticle of Scarab Beetles: 100 Years after Michelson. *Philos. Mag.* **2012**, *92*, 1583−1599.
(4) Barron, L. D. *Molecular Light Scattering and Optical Activity*; Cambridge University Press: Cambridge, 2004.
(5) Hiramatsu, K.; Okuno, M.; Kano, H.; Leproux, P.; Couderc, V.; Hamaguchi, H. Observation of Raman Optical Activity by Heterodyne-Detected Polarization-Resolved Coherent Anti-Stokes Raman Scattering. *Phys. Rev. Lett.* **2012**, *109*, 083901.
(6) Patterson, D.; Schnell, M.; Doyle, J. M. Enantiomer-Specific Detection of Chiral Molecules via Microwave Spectroscopy. *Nature* **2013**, *497*, 475−477.
(7) Tang, Y.; Cohen, A. E. Optical Chirality and Its Interaction with Matter. *Phys. Rev. Lett.* **2010**, *104*, 163901.
(8) Tang, Y.; Cohen, A. E. Enhanced Enantioselectivity in Excitation of Chiral Molecules by Superchiral Light. *Science* **2011**, *332*, 333−336.
(9) Govorov, A. O.; Gun'ko, Y. K.; Slocik, J. M.; Gérard, V. A.; Fan, Z.; Naik, R. R. Chiral Nanoparticle Assemblies: Circular Dichroism, Plasmonic Interactions, and Exciton Effects. *J. Mater. Chem.* **2011**, *21*, 16806.
(10) Ben-Moshe, A.; Maoz, B. M.; Govorov, A. O.; Markovich, G. Chirality and Chiroptical Effects in Inorganic Nanocrystal Systems with Plasmon and Exciton Resonances. *Chem. Soc. Rev.* **2013**, *42*, 7028−7041.
(11) Valev, V. K.; Baumberg, J. J.; Sibilia, C.; Verbiest, T. Chirality and Chiroptical Effects in Plasmonic Nanostructures: Fundamentals, Recent Progress, and Outlook. *Adv. Mater.* **2013**, *25*, 2517−2534.
(12) Papakostas, A.; Potts, A.; Bagnall, D.; Prosvirnin, S.; Coles, H.; Zheludev, N. Optical Manifestations of Planar Chirality. *Phys. Rev. Lett.* **2003**, *90*, 107404.
(13) Fedotov, V.; Mladyonov, P.; Prosvirnin, S.; Rogacheva, A.; Chen, Y.; Zheludev, N. Asymmetric Propagation of Electromagnetic Waves through a Planar Chiral Structure. *Phys. Rev. Lett.* **2006**, *97*, 1−4.
(14) Gansel, J. K.; Thiel, M.; Rill, M. S.; Decker, M.; Bade, K.; Saile, V.; von Freymann, G.; Linden, S.; Wegener, M. Gold Helix Photonic Metamaterial as Broadband Circular Polarizer. *Science* **2009**, *325*, 1513−1515.
(15) Dietrich, K.; Lehr, D.; Helgert, C.; Tünnermann, A.; Kley, E.-B. Circular Dichroism from Chiral Nanomaterial Fabricated by On-Edge Lithography. *Adv. Mater.* **2012**, *24*, 321−325.
(16) Rogacheva, A. V.; Fedotov, V. A.; Schwanecke, A. S.; Zheludev, N. I. Giant Gyrotropy due to Electromagnetic-Field Coupling in a Bilayered Chiral Structure. *Phys. Rev. Lett.* **2006**, *97*, 1−4.
(17) Esposito, M.; Tasco, V.; Todisco, F.; Benedetti, A.; Sanvitto, D.; Passaseo, A. Three Dimensional Chiral Metamaterial Nanospirals in the Visible Range by Vertically Compensated Focused Ion Beam Induced-Deposition. *Adv. Opt. Mater.* **2014**, *2*, 154−161.
(18) Hentschel, M.; Schäferling, M.; Weiss, T.; Liu, N.; Giessen, H. Three-Dimensional Chiral Plasmonic Oligomers. *Nano Lett.* **2012**, *12*, 2542−2547.
(19) Frank, B.; Yin, X.; Schäferling, M.; Zhao, J.; Hein, S. M.; Braun, P. V.; Giessen, H. Large-Area 3D Chiral Plasmonic Structures. *ACS Nano* **2013**, *7*, 6321−6329.
(20) He, Y.; Larsen, G. K.; Ingram, W.; Zhao, Y. Tunable Three-Dimensional Helically Stacked Plasmonic Layers on Nanosphere Monolayers. *Nano Lett.* **2014**, *14*, 1976−1981.
(21) Behar-Levy, H.; Neumann, O.; Naaman, R.; Avnir, D. Chirality Induction in Bulk Gold and Silver. *Adv. Mater.* **2007**, *19*, 1207−1211.
(22) Li, Z.; Zhu, Z.; Liu, W.; Zhou, Y.; Han, B.; Gao, Y.; Tang, Z. Reversible Plasmonic Circular Dichroism of Au Nanorod and DNA Assemblies. *J. Am. Chem. Soc.* **2012**, *134*, 3322−3325.
(23) Guerrero-Martínez, A.; Auguié, B.; Alonso-Gómez, J. L.; Džolić, Z.; Gómez-Graña, S.; Žinić, M.; Cid, M. M.; Liz-Marzán, L. M. Intense Optical Activity from Three-Dimensional Chiral Ordering of Plasmonic Nanoantennas. *Angew. Chem., Int. Ed.* **2011**, *50*, 5499−5503.
(24) Kuzyk, A.; Schreiber, R.; Fan, Z.; Pardatscher, G.; Roller, E.-M.; Högele, A.; Simmel, F. C.; Govorov, A. O.; Liedl, T. DNA-Based Self-Assembly of Chiral Plasmonic Nanostructures with Tailored Optical Response. *Nature* **2012**, *483*, 311−314.
(25) George, J.; Thomas, K. G. Surface Plasmon Coupled Circular Dichroism of Au Nanoparticles on Peptide Nanotubes. *J. Am. Chem. Soc.* **2010**, *132*, 2502−2503.
(26) Schreiber, R.; Luong, N.; Fan, Z.; Kuzyk, A.; Nickels, P. C.; Zhang, T.; Smith, D. M.; Yurke, B.; Kuang, W.; Govorov, A. O.; Liedl, T. Chiral Plasmonic DNA Nanostructures with Switchable Circular Dichroism. *Nat. Commun.* **2013**, *4*, 2948.
(27) Song, C.; Blaber, M. G.; Zhao, G.; Zhang, P.; Fry, H. C.; Schatz, G. C.; Rosi, N. L. Tailorable Plasmonic Circular Dichroism Properties of Helical Nanoparticle Superstructures. *Nano Lett.* **2013**, *13*, 3256−3261.
(28) Abdulrahman, N. a; Fan, Z.; Tonooka, T.; Kelly, S. M.; Gadegaard, N.; Hendry, E.; Govorov, A. O.; Kadodwala, M. Induced Chirality through Electromagnetic Coupling between Chiral Molecular Layers and Plasmonic Nanostructures. *Nano Lett.* **2012**, *12*, 977−983.
(29) Lu, F.; Tian, Y.; Liu, M.; Su, D.; Zhang, H.; Govorov, A. O.; Gang, O. Discrete Nanocubes as Plasmonic Reporters of Molecular Chirality. *Nano Lett.* **2013**, *13*, 3145−3151.
(30) Moskovits, M. Surface-Enhanced Spectroscopy. *Rev. Mod. Phys.* **1985**, *57*, 783−826.
(31) Anker, J. N.; Hall, W. P.; Lyandres, O.; Shah, N. C.; Zhao, J.; Van Duyne, R. P. Biosensing with Plasmonic Nanosensors. *Nat. Mater.* **2008**, *7*, 442−453.
(32) Abdali, S. Observation of SERS Effect in Raman Optical Activity, a New Tool for Chiral Vibrational Spectroscopy. *J. Raman Spectrosc.* **2006**, *37*, 1341−1345.
(33) Chulhai, D. V.; Jensen, L. Simulating Surface-Enhanced Raman Optical Activity Using Atomistic Electrodynamics-Quantum Mechanical Models *J. Phys. Chem. A* **2014**, doi: 10.1021/jp502107f.
(34) Hendry, E.; Carpy, T.; Johnston, J.; Popland, M.; Mikhaylovskiy, R. V.; Lapthorn, a. J.; Kelly, S. M.; Barron, L. D.; Gadegaard, N.; Kadodwala, M. Ultrasensitive Detection and Characterization of Biomolecules Using Superchiral Fields. *Nat. Nanotechnol.* **2010**, *5*, 783−787.
(35) Meinzer, N.; Hendry, E.; Barnes, W. L. Probing the Chiral Nature of Electromagnetic Fields Surrounding Plasmonic Nanostructures. *Phys. Rev. B* **2013**, *88*, 041407.
(36) Hendry, E.; Mikhaylovskiy, R. V.; Barron, L. D.; Kadodwala, M.; Davis, T. J. Chiral Electromagnetic Fields Generated by Arrays of Nanoslits. *Nano Lett.* **2012**, *12*, 3640−3644.
(37) Schäferling, M.; Dregely, D.; Hentschel, M.; Giessen, H. Tailoring Enhanced Optical Chirality: Design Principles for Chiral Plasmonic Nanostructures. *Phys. Rev. X* **2012**, *2*, 031010.
(38) García-Etxarri, A.; Dionne, J. a. Surface-Enhanced Circular Dichroism Spectroscopy Mediated by Nonchiral Nanoantennas. *Phys. Rev. B* **2013**, *87*, 235409.
(39) Schäferling, M.; Yin, X.; Engheta, N.; Giessen, H. Helical Plasmonic Nanostructures as Prototypical Chiral Near-Field Sources. *ACS Photonics* **2014**, *1*, 530−537.
(40) Fredriksson, H.; Alaverdyan, Y.; Dmitriev, A.; Langhammer, C.; Sutherland, D. S.; Zäch, M.; Kasemo, B. Hole−Mask Colloidal Lithography. *Adv. Mater.* **2007**, *19*, 4297−4302.
(41) Fan, Z.; Zhang, H.; Govorov, A. O. Optical Properties of Chiral Plasmonic Tetramers: Circular Dichroism and Multipole Effects. *J. Phys. Chem. C* **2013**, *117*, 14770−14777.

(42) Hentschel, M.; Wu, L.; Schäferling, M.; Bai, P.; Li, E. P.; Giessen, H. Optical Properties of Chiral Three-Dimensional Plasmonic Oligomers at the Onset of Charge-Transfer Plasmons. *ACS Nano* **2012**, *6*, 10355−10365.
(43) Hentschel, M.; Schäferling, M.; Metzger, B.; Giessen, H. Plasmonic Diastereomers: Adding up Chiral Centers. *Nano Lett.* **2013**, *13*, 600−606.
(44) Xu, H.; Bjerneld, E.; Käll, M.; Börjesson, L. Spectroscopy of Single Hemoglobin Molecules by Surface Enhanced Raman Scattering. *Phys. Rev. Lett.* **1999**, *83*, 4357−4360.
(45) Tong, L.; Xu, H.; Käll, M. Nanogaps for SERS Applications. *MRS Bull.* **2014**, *39*, 163−168.
(46) Nair, G.; Singh, H. J.; Paria, D.; Venkatapathi, M.; Ghosh, A. Plasmonic Interactions at Close Proximity in Chiral Geometries: Route toward Broadband Chiroptical Response and Giant Enantiomeric Sensitivity. *J. Phys. Chem. C* **2014**, *118*, 4991−4997.
(47) Shegai, T.; Chen, S.; Miljković, V. D.; Zengin, G.; Johansson, P.; Käll, M. A Bimetallic Nanoantenna for Directional Colour Routing. *Nat. Commun.* **2011**, *2*, 481.
(48) Shegai, T.; Johansson, P.; Langhammer, C.; Käll, M. Directional Scattering and Hydrogen Sensing by Bimetallic Pd-Au Nanoantennas. *Nano Lett.* **2012**, *12*, 2464−2469.
(49) Schwind, M.; Miljković, V. D.; Gusak, V.; Käll, M.; Zorić, I.; Johansson, P. Diffraction from Arrays of Plasmonic Lateral Order. *ACS Nano* **2012**, *6*, 9455−9465.
(50) Svedendahl, M.; Käll, M. Fano Interference between Localized Plasmons and Interface Reflections. *ACS Nano* **2012**, *6*, 7533−7539.
(51) Wang, R.-Y.; Wang, H.; Wu, X.; Ji, Y.; Wang, P.; Qu, Y.; Chung, T.-S. Chiral Assembly of Gold Nanorods with Collective Plasmonic Circular Dichroism Response. *Soft Matter* **2011**, *7*, 8370.
(52) Kosaka, Y.; Egami, K.; Tomita, S.; Yanagi, H. Plasmonic Circular Dichroism Using Au Fine Particles and Riboflavin. *Phys. Status Solidi* **2012**, *9*, 2529−2532.
(53) Johnson, P. B.; Christy, R. W. Optical Constants of the Noble Metals. *Phys. Rev. B* **1972**, *6*, 4370−4379.
(54) Jensen, T.; Kelly, L.; Lazarides, A.; Schatz, G. C. Electrodynamics of Noble Metal Nanoparticles and Nanoparticle Clusters. *J. Cluster Sci.* **1999**, *10*, 295−317.